Supplemental Information for:

Potent immune stimulation from nanoparticle carriers relies on the interplay of adjuvant surface density and adjuvant mass distribution

*Jeffery Noble, Anthony Zimmerman, Catherine A. Fromen**

Department of Chemical Engineering, University of Michigan, Ann Arbor, MI 48109.

*Corresponding author: Catherine A. Fromen, Department of Chemical Engineering, University of Michigan, NCRC B028/Rm. G029E, 2800 Plymouth Road, Ann Arbor, MI 48109, Telephone: (734) 763-7807, cfromen@umich.edu

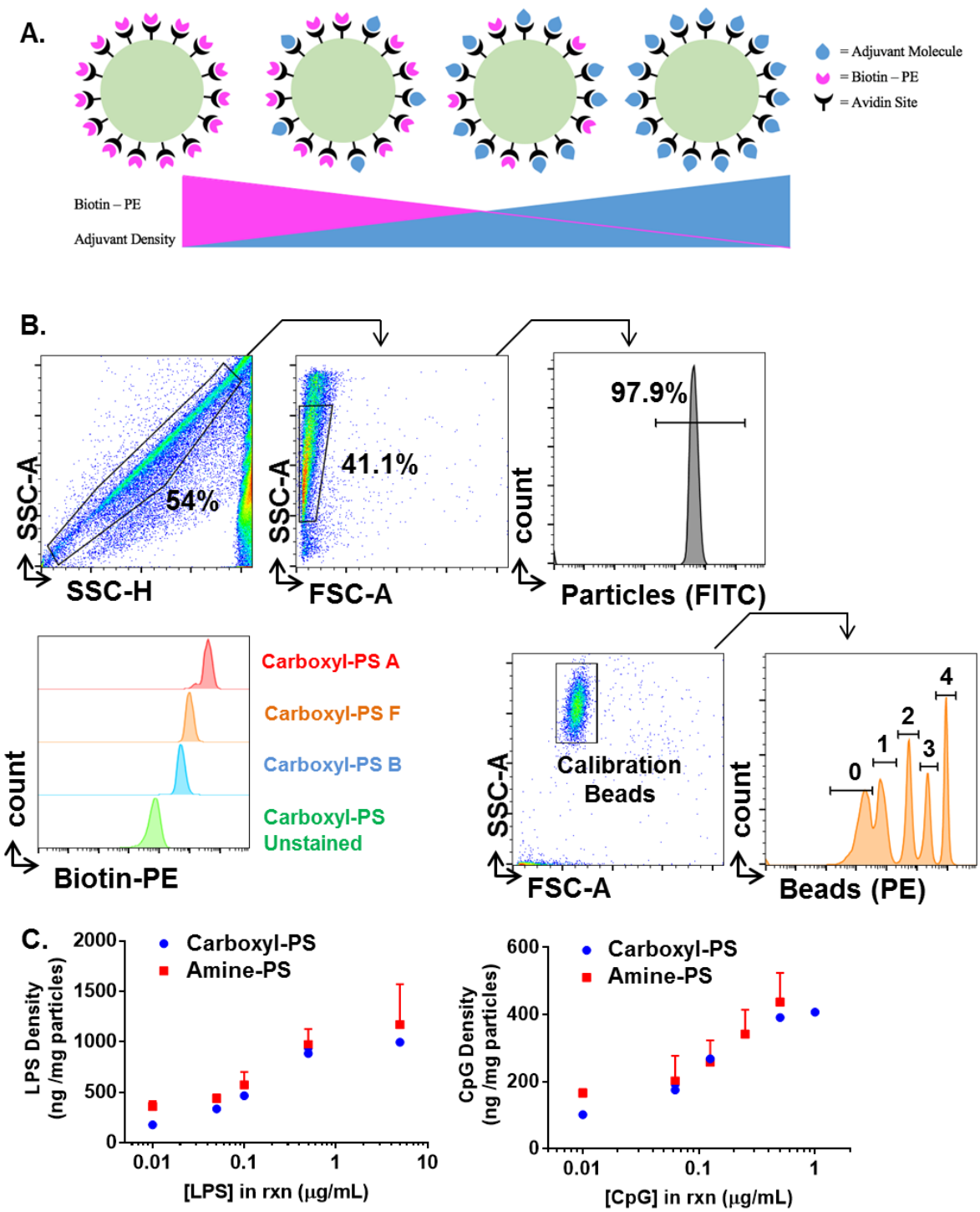

Figure S1. (A) Diagram of backfill quantification approach to determine adjuvant ligand densities (B) Representative flow cytometry gating for 500 nm particles (carboxyl-PS shown) and calibration beads used to convert median fluorescent intensity (MFI) values to Molecules of Soluble Fluorochrome (MESF) units and subsequent molecules per particle. (C) Reaction conditions for LPS and CpG particle functionalization. N=5 independent particle batches, error bars represent standard error.

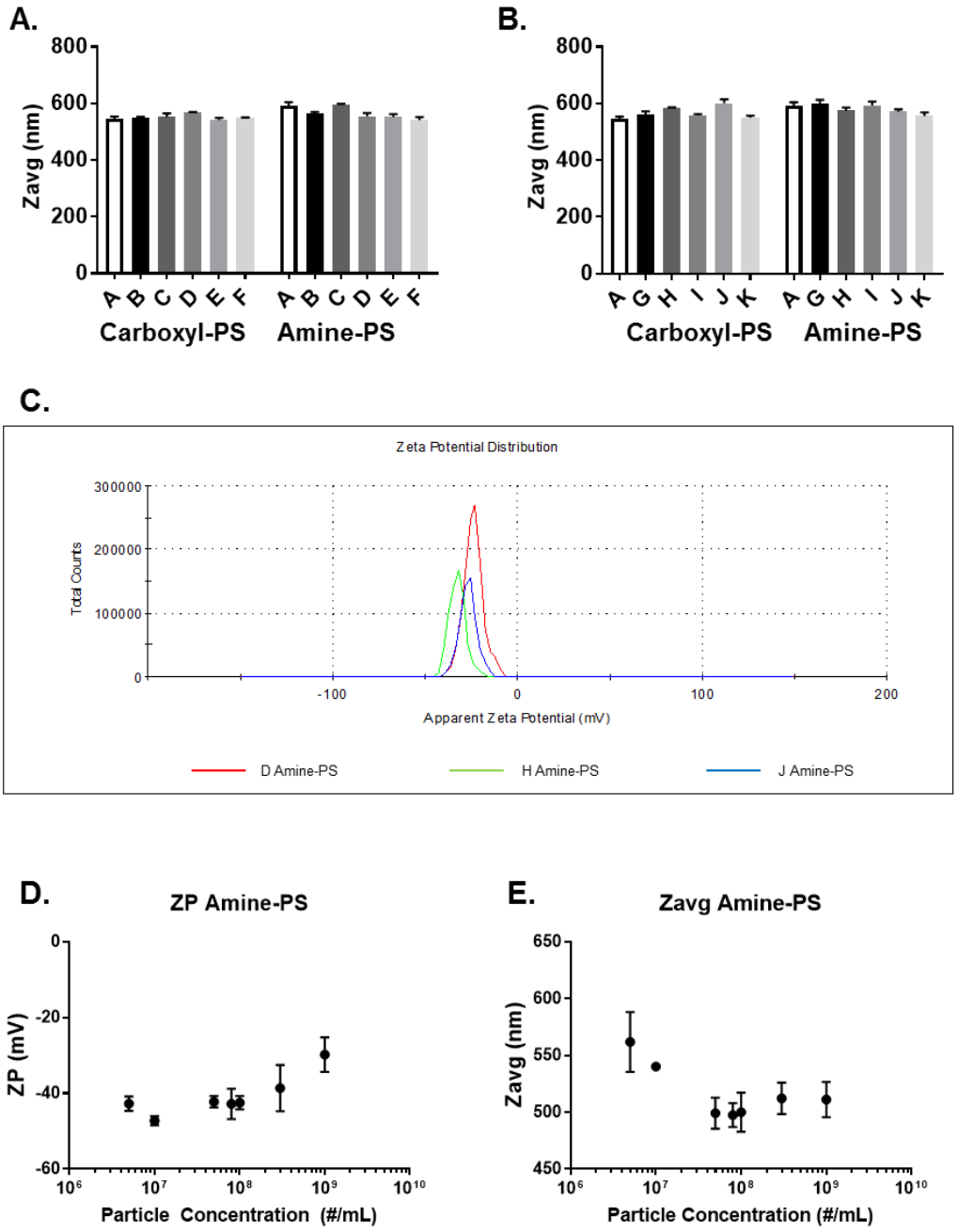

Figure S2. Hydrodynamic diameter Z average (Zavg) measurements from DLS (A) LPS-modified particles and (B) CpG-modified particles. Representative results from a single particle batch, error bars represent standard error. (C) Representative zeta potential distributions of three amine-PS particle samples. (D) Zeta potential (ZP) and (E) Zavg measurements of unmodified amine-PS particles at varied concentrations prior to avidin modification.

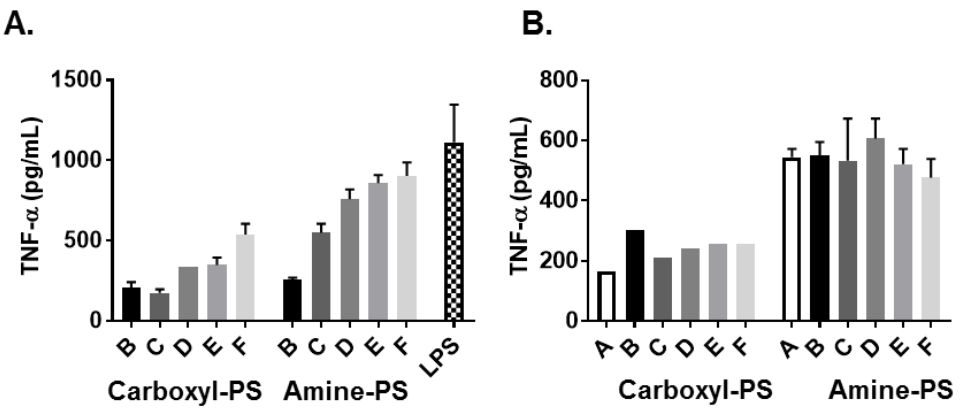

Figure S3. TNF-α Production from C57BL/6 BMMs at 24 hrs. Additional proinflammatory cytokine TNF-α demonstrating similar trends to the representative IL-6 production when dosed at (A) constant LPS dosage [25 ng/mL] and (B) equivalent particle concentration [$1x10^7$ particles/mL] with varying dosages of LPS. Data correspond to IL-6 results from (A) Figure 2A and (B) Figure 2C.

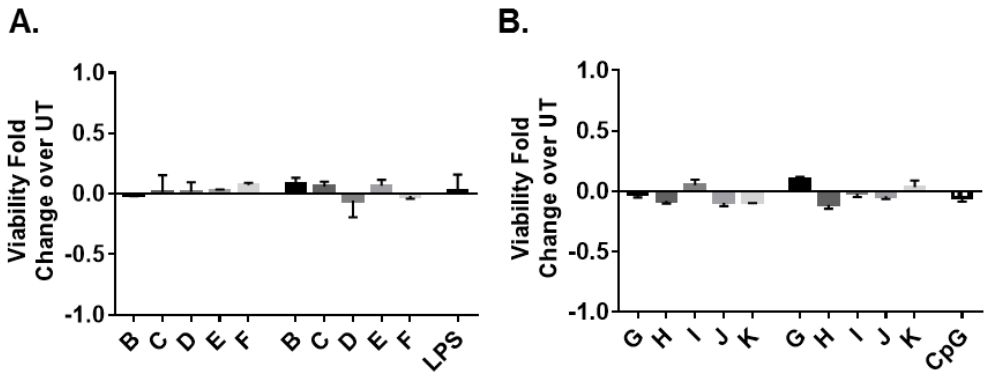

Figure S4. Cell viability assay results for BMMs following (A) LPS and (B) CpG equivalent adjuvant dosing.

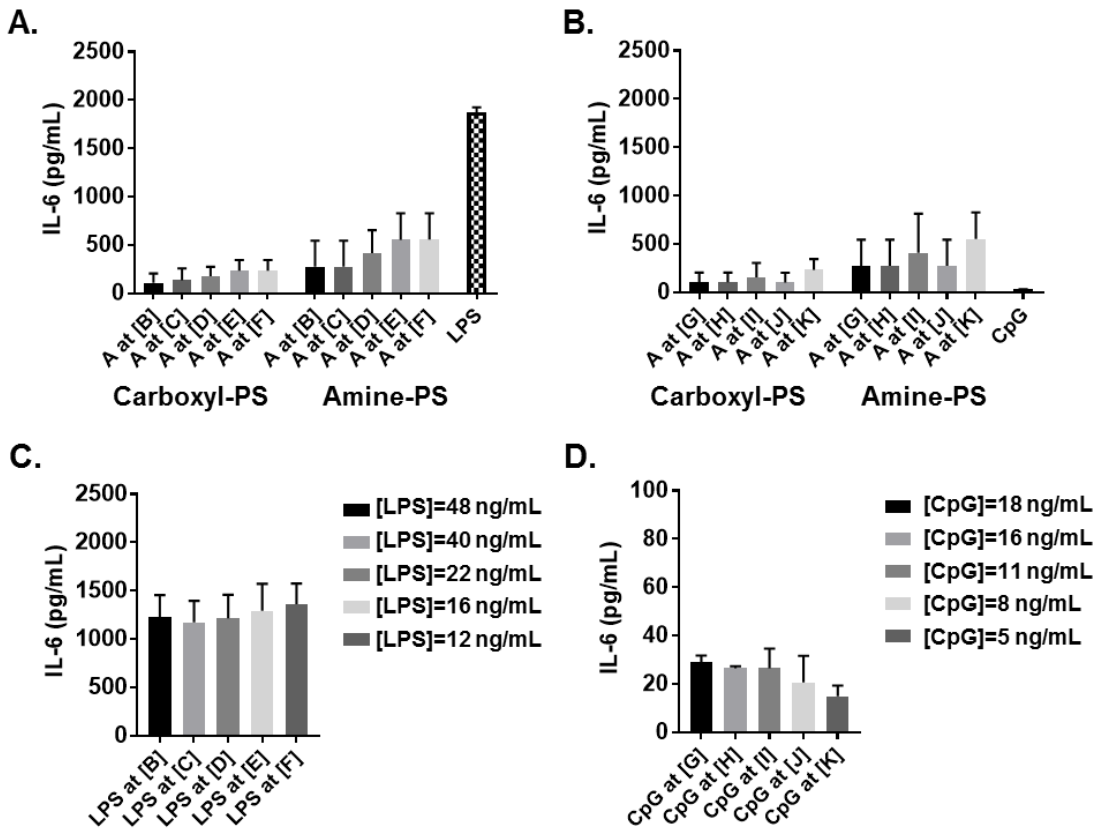

Figure S5. IL-6 production of corresponding controls from C57BL/6 BMMs at 24 hrs. Particle incubation of avidin-modified, adjuvant-free particles A at particle concentrations corresponding to functionalized particle dosing at (A) constant LPS dosage [25 ng/mL] (as shown in Figure 2A) and (B) constant CpG dosage [10 ng/mL] (as shown in Figure 2B). Soluble adjuvant incubation of (C) LPS (as shown in Figure 2C) and (D) CpG (as shown in Figure 2D) dosed at adjuvant concentrations corresponding to the equivalent particle dosing [$1x10^7$ particles/mL] which resulted in varied dosages of adjuvant.

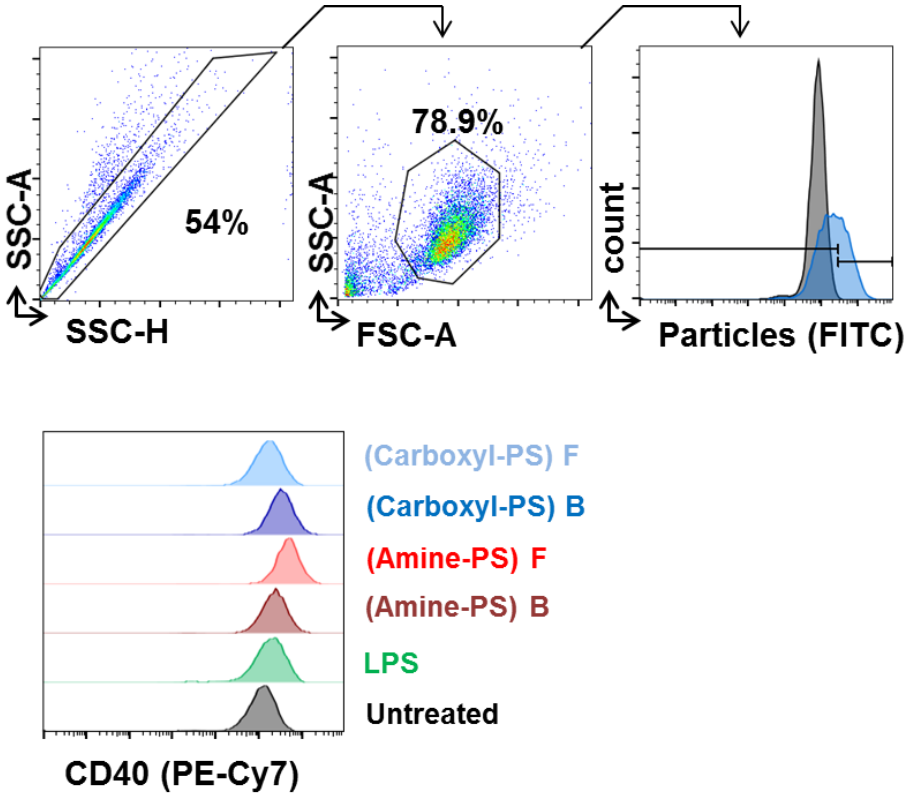

Figure S6. Representative flow cytometry for BMM cell identification from Figures 3-4. BMMs were gated as singles using SSC-A vs SSC-H and identified using their FSC and SSC. Initial fluorescence gates for particle internalization was set using untreated controls, with particle positive cells identified with a shift in fluorescence intensity in the FITC channel. Non-fluorescent amine-PS particles were stained with biotin-FITC following adjuvant conjugation immediately prior to dosing. MFI values for CD40 (shown above), CD80 and CD86 were determined for the entire population, as well as particle positive cells. In all graphs, gray curves represent untreated samples, blue curves represent samples receiving $1x10^7$/mL carboxyl-PS particles.

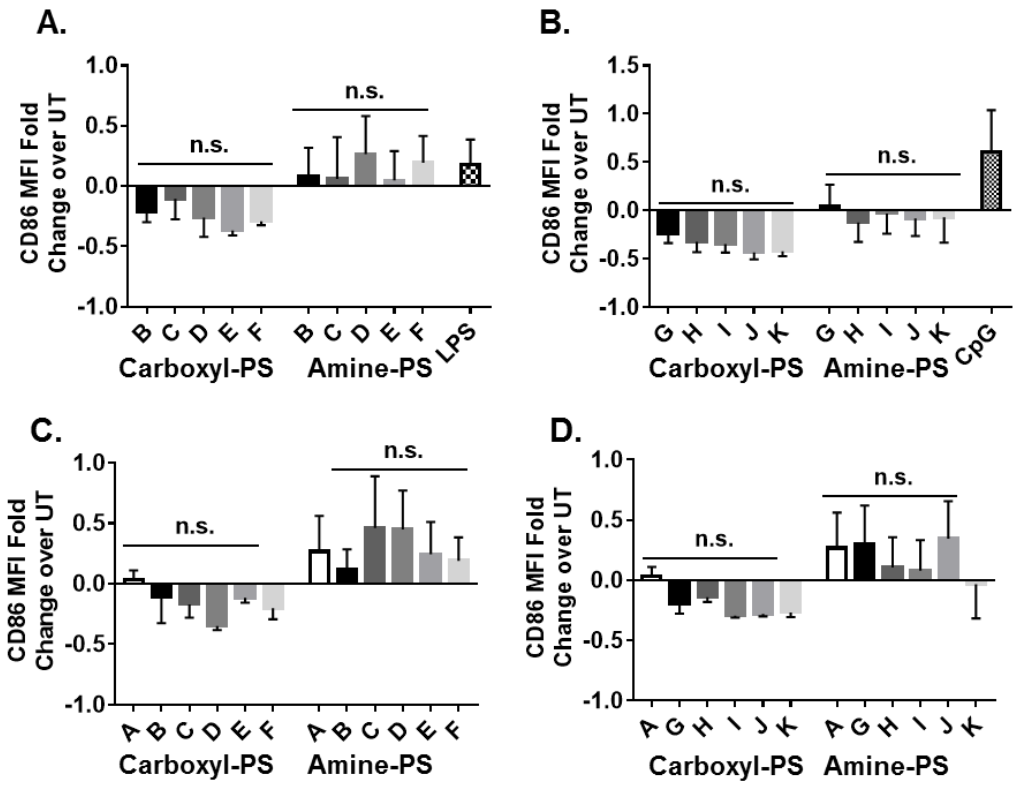

Figure S7. Fold Change of CD86 Costimulatory Molecule Expression from BMMs. BMM fold expression of CD86 from incubation with (A) LPS and (B) CpG conjugated nanoparticles at equivalent adjuvant concentration. BMM fold expression of CD86 from incubation with (C) LPS and (D) CpG conjugated nanoparticles at constant particle concentration. Equivalent adjuvant doses of either 25 ng/mL LPS or 10 ng/mL CpG; equivalent particle concentration $1x10^7$/mL. Incubation performed for 24 hr. Standard error shown. Statistical analysis performed by two-way ANOVA with Tukey's multiple comparisons, non-significant. Representative results from single experiment, error bars represent standard error of technical replicates (N=3).

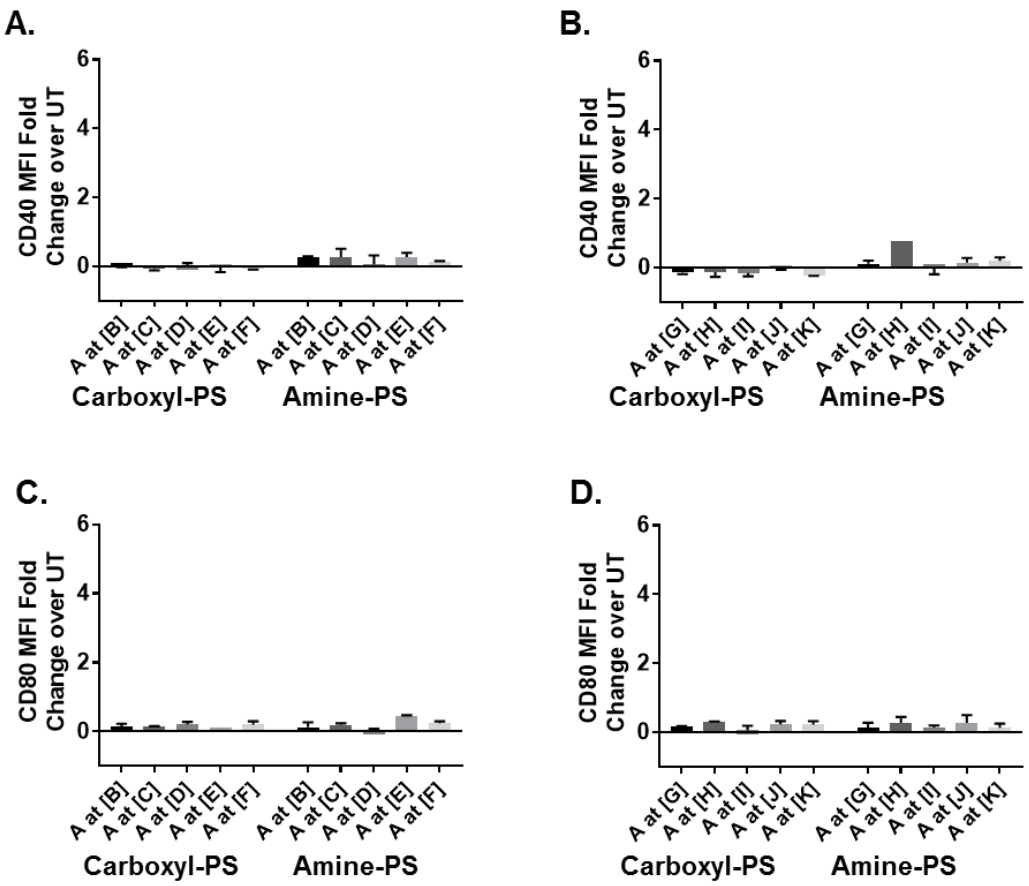

Figure S8. Fold changes of costimulatory molecule expression of corresponding controls from BMMs at a constant adjuvant dose. BMM fold expression of (A and B) CD40 and (C and D) CD80 following particle incubation of avidin-modified, adjuvant-free particles A at particle concentrations corresponding to functionalized particle dosing at constant adjuvant of Figure 3. (A and C) LPS dosage [25 ng/mL] (as shown in Figure 3A and C) and (B and D) constant CpG dosage [10 ng/mL] (as shown in Figure 2B). Representative results from single experiment, error bars represent standard error of technical replicates (N=3).

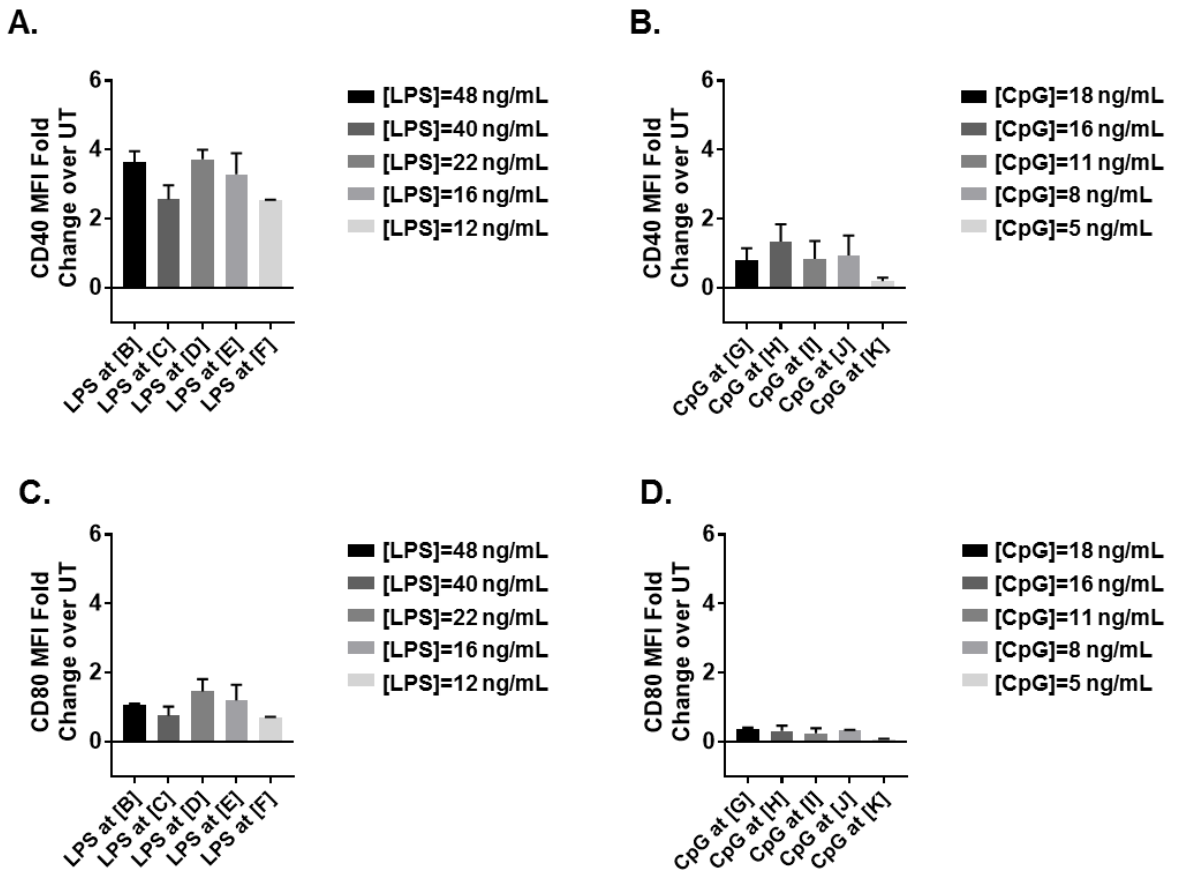

Figure S9. Fold changes of costimulatory molecule expression of corresponding controls from BMMs at a constant particle dose. Soluble adjuvant incubation dosed at adjuvant concentrations corresponding to the equivalent particle dosing [$1x10^7$ particles/mL] of Figure 4. BMM fold expression of CD40 from incubation with (A) LPS and (B) CpG equivalence. BMM fold expression of CD80 from incubation with (C) LPS and (D) CpG equivalence. Representative results from single experiment, error bars represent standard error of technical replicates (N=3).

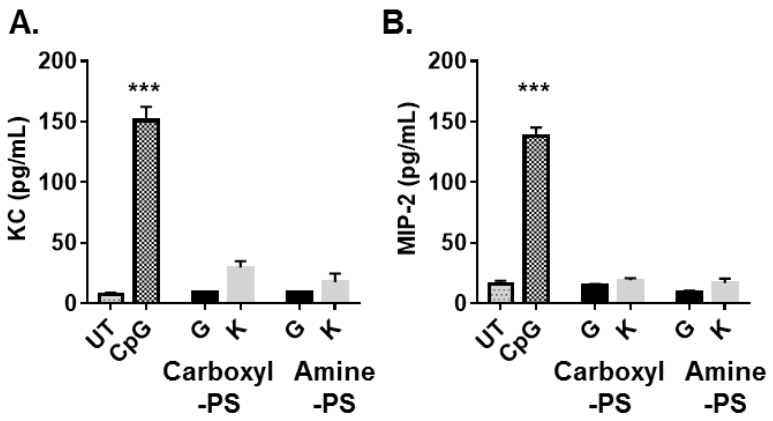

Figure S10. BALF Cytokine Production Following Pulmonary Instillation at Constant CpG Dose. KC and MIP-2 cytokine concentrations measured in the BALF of C57BL/6 mice 24 hrs post pulmonary instillation in mice dosed with equivalent dose of CpG (2.5 µg/mouse). Statistical analysis performed by one-way ANOVA with Dunnett's multiple comparisons test. Stars indicate significant differences between UT *** $p<0.001$. N=5 mice, Standard error is shown.

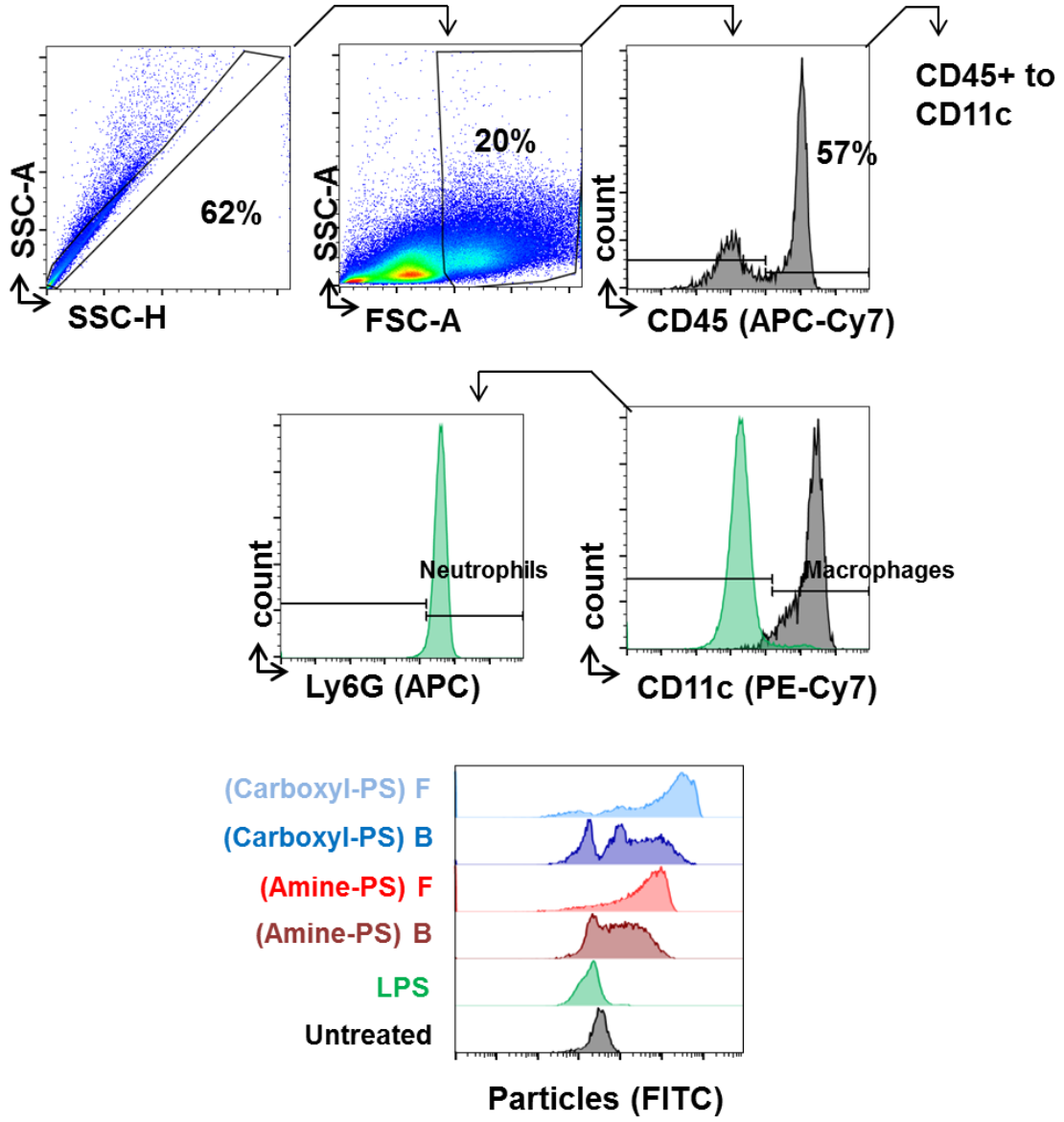

Figure S11. Representative Gating for BALF lung cells from Figure 6. BALF cells were gated as singles using SSC-A vs SSC-H and identified using their FSC and SSC. Initial fluorescence gates were set using fluorescence minus one (FMO) controls. BALF cells were then identified as CD45+ and gated on CD11c, with BALF macrophages identified as CD45+/CD11c+. From the CD11c- population, BALF neutrophils were confirmed to be Ly6G+. From the overall BALF count and each leukocyte population, particle positive cells were identified as FITC+.

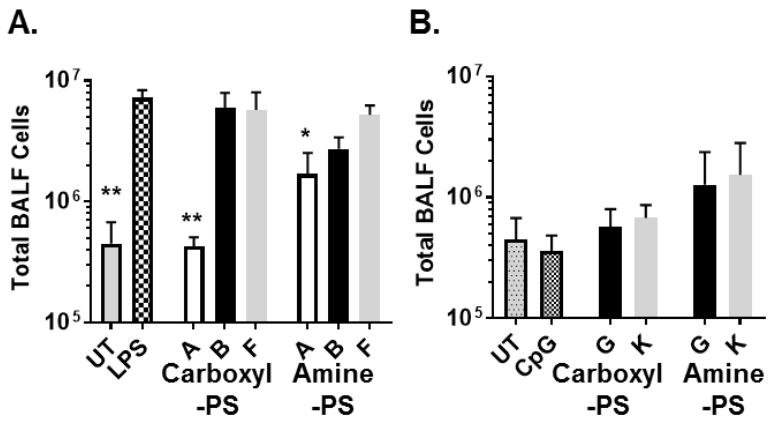

Figure S12. Total BALF cells via hemacytometer. Statistical analysis performed by a one-way ANOVA with Dunnett's multiple comparisons test. Representative results from single experiment, N=5 mice, standard error is shown. Stars indicate significant differences between UT *p<0.05, ** p<0.01, *** p<0.001.

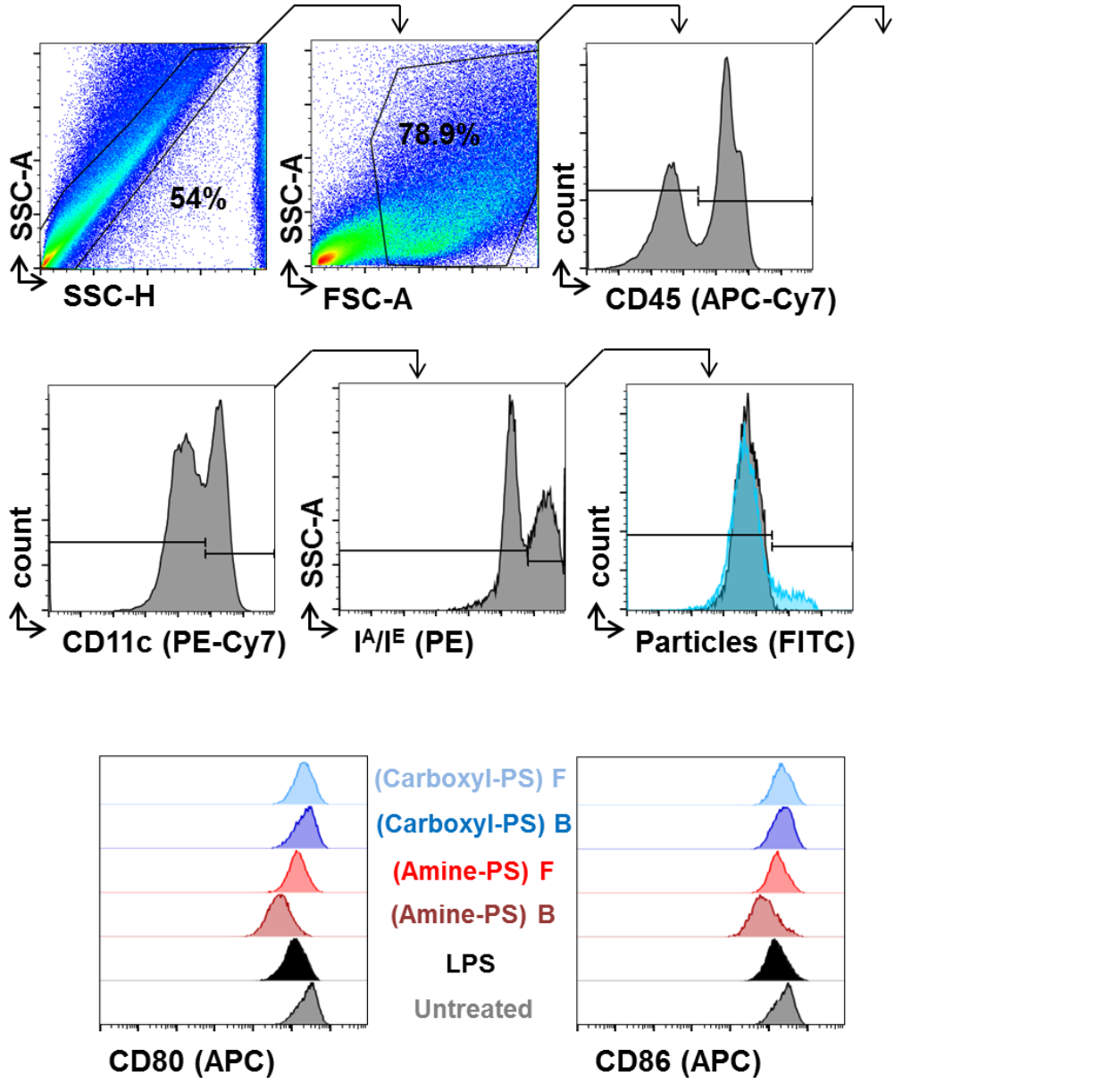

Figure S13. Representative Gating for the Lung. Cells were gated as singles using SSC-A vs SSC-H and leukocytes using SSC-A vs FSC-A and CD45+. Lung dendritic cells (DCs) were then identified as CD11c+ and I^A/I^E $(MHC\ II)^{hi}$. Particle positive DCs were identified using a positive signal in the FITC channel. Within each population, MFI for CD80 and CD86 were determined (lung cells divided into multiple panels prior to staining).

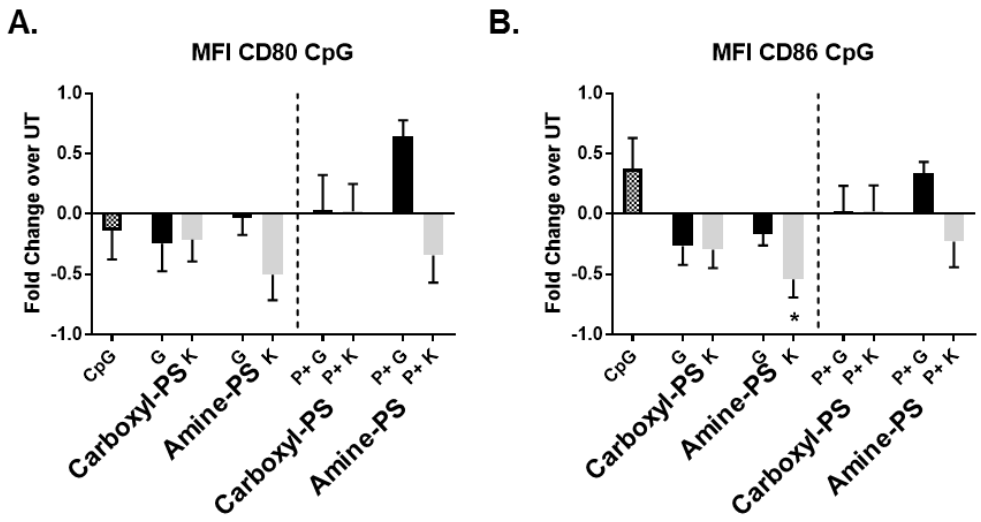

Figure S14. Fold changes in MFI for CD80 and CD86 following CpG dosing.

SUPPLEMENTAL TABLES

Table S1. Characterization of Adjuvant-Conjugated Nanoparticles. Particle types A – K with corresponding particle characteristics. Adjuvant ligand density represented as both a numerical density (numbers of molecules/surface area) and a mass density (ng adjuvant/mg particle). Numerical adjuvant density values determined via flow cytometry through the backfill method (Supp. Fig. 1.), n ≥ 5 particle batches, mean and standard error shown.

Particle	Adjuvant	Surface Charge	Zavg (nm)	ZP (mV)	Adjuvant Density	
					(#/μm^2)	ng/mg
A	-	Carboxyl-PS	545 ± 15	-32.0 ± 0.6	-	-
		Amine-PS	592 ± 22	-23.6 ± 0.5	-	-
B	LPS	Carboxyl-PS	550 ± 5	-20.7 ± 1.5	5.54e4 ± 1800	996.0 ± 33
		Amine-PS	566 ± 8	-21.4 ± 0.1	6.52e4 ± 17000	1171.1 ± 309
C	LPS	Carboxyl-PS	552 ± 22	-23.7 ± 0.5	4.92e4 ± 2200	883.5 ± 40
		Amine-PS	594 ± 9	-20.9 ± 0.3	5.42e4 ± 7600	972.8 ± 137
D	LPS	Carboxyl-PS	567 ± 5	-23.1 ± 0.7	2.60e4 ± 600	466.6 ± 11
		Amine-PS	555 ± 21	-21.7 ± 0.9	3.2e4 ± 7000	574.4 ± 126
E	LPS	Carboxyl-PS	542 ± 13	-21.0 ± 0.6	1.87e4 ± 2100	335.6 ± 38
		Amine-PS	552 ± 19	-18.4 ± 0.2	2.44e4 ± 2000	438.6 ± 37
F	LPS	Carboxyl-PS	548 ± 4	-23.0 ± 0.3	9.92e3 ± 1100	178.1 ± 20
		Amine-PS	542 ± 17	-19.6 ± 0.3	2.00e4 ± 2200	359.3 ± 40
G	CpG	Carboxyl-PS	563 ± 17	-30.1 ± 0.9	5.33e4 ± 1300	407.2 ± 10
		Amine-PS	600 ± 23	-31.2 ± 0.3	5.72e4 ± 11000	437.3 ± 87
H	CpG	Carboxyl-PS	584 ± 5	-29.5 ± 0.1	5.12e4 ± 1400	391.1 ± 10
		Amine-PS	575 ± 19	-32.8 ± 0.5	4.47e4 ± 9400	341.9 ± 72
I	CpG	Carboxyl-PS	558 ± 9	-29.1 ± 0.2	3.51e4 ± 1400	268.4 ± 10
		Amine-PS	594 ± 23	-28.7 ± 0.7	3.38e4 ± 8500	258.4 ± 65
J	CpG	Carboxyl-PS	601 ± 23	-23.5 ± 0.3	2.29e4 ± 1600	175.3 ± 13
		Amine-PS	546 ± 14	-16.0 ± 2.5	2.65e4 ± 9700	202.3 ± 75
K	CpG	Carboxyl-PS	550 ± 12	-23.5 ± 0.6	1.33e4 ± 400	101.8 ± 3
		Amine-PS	557 ± 20	-18.7 ± 1.2	2.17e4 ± 1400	165.7 ± 11